Journal of Control, Automation and Electrical Systems (2018) 29:460–469
https://doi.org/10.1007/s40313-018-0380-0

Attitude, Angle of Attack and Angle of Sideslip Determination Using Carrier Phase Integer Ambiguity Estimation

R. de F. E. Campos[1] · E. M. Hemerly[1]

Received: 5 February 2018 / Revised: 5 March 2018 / Accepted: 8 March 2018 / Published online: 10 May 2018

Abstract
The Global Navigation Satellite System (GNSS) positioning solution may be computed to a cm level of error, if the signal carrier phase is properly considered during the calculations. With such a precision, even attitude angles can be precisely estimated if more than one antennae is available. However, using the carrier phase information depends on solving the carrier phase integer ambiguity problem which is intrinsic to this approach. Since only a fraction of the carrier phase is observed by the GNSS receivers, the solution for the integer ambiguity is usually obtained by means of search algorithms, based on least squares. This contribution investigates the performance of the integer ambiguity solution for the attitude determination problem and also proposes a novel application: angle of attack and angle of sideslip estimation for specific aeronautical application. This novel application benefits aeronautical industry by introducing a new alternative for measuring reliable airdata parameters, namely angle of attack and angle of sideslip, by using a nonsusceptible to icing conditions data. The results presented here are based on the constrained LAMBDA method. Dynamic real data are used for evaluation of the proposed novel application.

Keywords Attitude determination · Angle of attack · Angle of sideslip · GNSS positioning · Carrier phase integer ambiguity · C-LAMBDA

1 Introduction

The navigation solution consists in determining an object position and attitude along time. In the case of inertial navigation systems, the solution is obtained based on sensors which do not depend on external inputs. In such a condition, due to the inertial sensors errors, the navigation solution uncertainty increases indefinitely along time. To avoid this behavior, external sensors are required, so that when their inputs are available, it is guaranteed that the uncertainty is limited to the external sensors accuracy, independently of the system operation time (Farrel and Barth 1999; Groves 2008; Hermerly and Schad 2004; Titterton and Weston 1997).

Many navigation algorithms in the literature describe methods to maintain the solution accuracy, even in the presence of sensors errors (Bar-Itzhack 1977; de F. E. Campos 2011; Savage 1998a, b). However, the solution quality will directly depend on the sensors accuracy and availability. In application which requires high-accuracy, high-cost sensors are required, which may cause the solution to be nonviable. Currently, GNSS is a low-cost, high-accuracy alternative for this kind of problem.

As summarized in Kim and Langley (2000), Chang and Zhou (2006), many contributions have being published in the last decades considering the GNSS carrier phase application for low-cost, very high-precision navigation solution. The following types of algorithms can be found in the literature: (a) C/A or P code based—which combines L1 and L2 pseudorange observations to determine ambiguities carrier phases ambiguities; (b) AFM (ambiguity function method)—considered the first single-epoch ambiguity resolution technique; (c) and the search-based techniques—which basically consists in three steps: float solution, integer ambiguity estimation, and fixed solution. The search-based algorithms essentially only differ from one another in terms of computational complexity. Examples of such methods are LSAST (Least-Squares Ambiguity Search Technique), FARA (Fast

✉ R. de F. E. Campos
renanpos@yahoo.com.br

E. M. Hemerly
emhemerly@uol.com.br

[1] Divisão de Engenharia Eletrônica, Depto. de Sistemas e Controle, Instituto Tecnológico de Aeronáutica, São José dos Campos, SP CEP 12.228-900, Brazil

Ambiguity Resolution Approach), MILES (Mixed Integer Least-Squares Method), Modified Cholesky Decomposition, Null Space, FASF (Fast Search Filter), OMEGA (Method of Estimating GPS Ambiguities), LAMBDA (Least-Squares Ambiguity Decorrelation Adjustment).

Position error in the order of centimeters can be achieved using the carrier phase information and a set of two or more GNSS antennae. With such a precision, even attitude solution can be precisely obtained; however, this requires the integer ambiguity solution to be available in real time or "on-the-fly" as usually described in the literature (Leik 1995; Hofmann-Wellenhof et al. 2001). In Hatch (1990), discussions regarding real-time application were introduced, but the computational resources available were yet very limited. In Teunissen (1994), Teunissen (2017), Jonge and Tiberius (1996), Verhagen (2005); Verhagen and Teunissen (2006), Chang and Zhou (2006), Wang et al. (2009), Li and Shen (2010), Giorge et al. (2010), the LAMBDA method was proposed and represented an important improvement in the solution reliability based on least squares. Improvements to the method were later introduced (constrained LAMBDA) as described in Teunissen (2007), Wang et al. (2009), Park and Teunissen (2009), Giorge et al. (2010), Giorge and Teunissen (2012). Baroni and Kuga (2009), Baroni and Kuga (2012) and Teunissen et al. (2011) evaluation on the ambiguity resolution methods, and applications for positioning and attitude determination are described in details. More recently investigations on the advantages of mixing several GNSS technologies from multiple countries, and considering several carrier frequencies, are under discussion for long ($>$ 10 km) and short ($<$ 10 km) baselines applications (Liu et al. 2016; Nadarajah et al. 2016; Quan et al. 2016).

The considerable efforts applied in the development of reliable GNSS carrier phase algorithms can also benefit the aeronautical industry, as will be demonstrated in the main contribution of this paper. In the past few years several incidents and accidents have been reported due to unreliable airdata caused icing conditions (Flottau 2010; Skybrary 2018). After the last reports, the main authorities FAA (Federal Aviation Administration) and EASA (European Aviation Safety Agency) initiated several investigations on the root cause of the failures. It was found that rare atmospheric icing conditions (such as ice crystals and supercooled large drops) are now being more easily found in nature. Figure 1 presents example of ice accretion in a typical pitot tube that could lead to unreliable airdata.

So, new and tighter certification requirements for airdata systems had to be released in order to keep the safety levels of the aeronautical segment (NPA 2012-22 2012; EDD 2015/08/R 2015; Sultan 2015). Other authorities worldwide usually update their certification basis a few months after FAA, and/or EASA releases their new requirements for the aircraft's manufacturers. Initially one alternative to

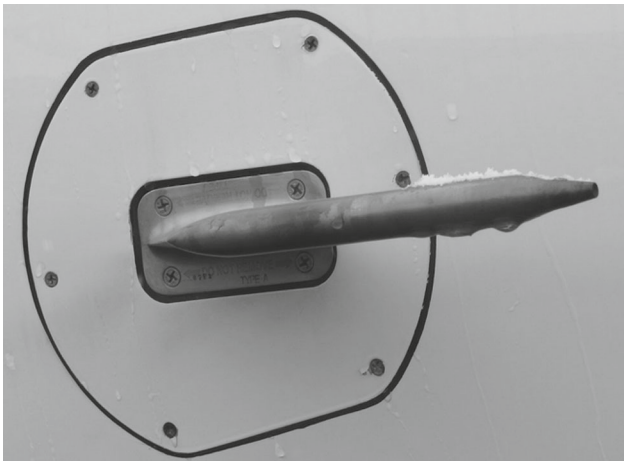

Fig. 1 Ice accretion in airdata system (Lopez 2016)

Fig. 2 Airbus A-350 Airdata Systems

comply with the more restrictive requirements for airdata systems consists in including additional redundant systems—see Airbus recently certified A-350 XW in Fig. 2. However, the inclusion of additional airdata systems considerably impacts the aircraft aerodynamics, maintainability, weight, and power consumption. (These equipments must include high-power heating capability in order to avoid icing conditions.) Each new system integration demands complex, multi-disciplinary, highly specialized manpower, and associated extensive certification tests (in laboratory, and on aircraft) besides the extensive amount of paperwork involved in the process.

In this contribution the C-LAMBDA (Teunissen et al. 2011) method will be applied for attitude determination and also for the novel aeronautical application to provide low-cost, zero weight, virtually zero power consuming, independent and dissimilar source of angle of attack and angle of sideslip. The results here presented introduce a relevant alternative for aeronautical industry to overcome the more restrictive certification requirements with considerably reduced certification costs and with essentially no impact to aircraft performance and maintainability.

The paper is organized as follows: Sect. 1 presents the introduction of the work here developed; Sect. 2 reviews the GNSS observation equations; Sect. 3 summarizes the C-LAMBDA method; Sect. 4 presents the attitude computation equations; in Sect. 5 the GNSS-based angle of attack and angle of sideslip equations are presented. The obtained results and observations are presented in Sect. 6. Conclusions are presented in Sect. 7.

2 GNSS Position Determination

The position solution computed based on code pseudorange triangulation is widely used in several civil applications, such as mobile phones, cars, ships, aircrafts, UAVs. The triangulation is usually performed by the GNSS receivers, using the open civil signals from each visible satellite. Although the obtained precision is acceptable for most of these applications—in the order of meters—this may not be true for some particular cases, for example, when attitude is being estimated based on GNSS data. In such a case, a precision in the order of centimeters may be required. This can be achieved using two or more GNSS antennae and the carrier phase information.

The position solution can be obtained, based on the known received GNSS carrier wavelength being captured, the measured (fractional) phase range, and the number of cycles propagated between the satellite and the receiver (ambiguity), as described in Fig. 3.

The distance between the satellites and the receiver's antennae can be precisely estimated based on the integer number of wavelengths that can be placed between them. This integer number is known as the integer phase ambiguity, and due to distortions and errors intrinsic to the GNSS design and environment, the integer ambiguity solution may be incorrectly estimated, causing the positioning errors to be increased.

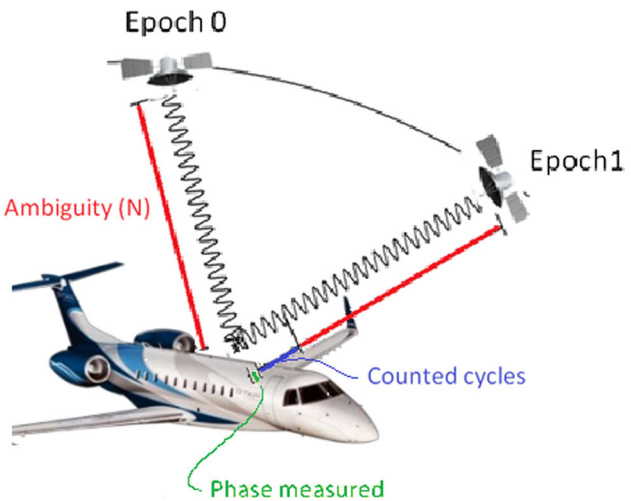

Fig. 3 GNSS carrier wavelength

As follows, (1) and (2) present the GNSS observation equations for the code pseudodistance and carrier phase measurement.

$$p_r^{\mathrm{S}}(t_r) = \rho_r^{\mathrm{S}}(t^{\mathrm{S}}) + c{\cdot}\mathrm{d}t_r - c.\mathrm{d}t^{\mathrm{S}} + I_r^{\mathrm{S}}(t_r) + T_r^{\mathrm{S}}(t_r) + d_r^{\mathrm{S}}(t_r) + e_r^{\mathrm{S}} \quad (1)$$

where

$p_{\mathrm{r}}^{\mathrm{S}}$ is the measured code pseudodistance (m);
t_{r} is the time when the transmitted signal arrived at receiver r (s);
$\rho_{\mathrm{r}}^{\mathrm{S}}$ is the geometric distance between satellite S and receiver r (m);
t^{S} is the time when the signal was transmitted from the satellite S (s);
c is the speed of light (m/s);
$\mathrm{d}t_{\mathrm{r}}$ is the receiver clock error for code data (s);
$\mathrm{d}t^{\mathrm{S}}$ is the satellite clock error for code data (s);
$I_{\mathrm{r}}^{\mathrm{S}}$ is the ionospheric induced error (m);
$T_{\mathrm{r}}^{\mathrm{S}}$ is the tropospheric induced error (m);
$d_{\mathrm{r}}^{\mathrm{S}}$ is the multi-path induced errors for code data (m);
$e_{\mathrm{r}}^{\mathrm{S}}$ is the code pseudodistance Gaussian, independent, zero mean random measurement noise (m)

$$\varphi_r^{\mathrm{S}}(t_r) = \frac{f}{c}\rho_r^{\mathrm{S}}(t^{\mathrm{S}}) + N_r^{\mathrm{S}} + f{\cdot}\delta t_r - f{\cdot}\delta t^{\mathrm{S}} - \frac{f}{c}I_r^{\mathrm{S}}(t_r) + \frac{f}{c}T_r^{\mathrm{S}}(t_r) + \frac{f}{c}\delta_r^{\mathrm{S}}(t_r) + \frac{f}{c}\varepsilon_r^{\mathrm{S}}(t_r) \quad (2)$$

where

$\varphi_{\mathrm{r}}^{\mathrm{S}}$ is the measured carrier phase [cycles];
f is the signal carrier frequency (Hz);
$N_{\mathrm{r}}^{\mathrm{S}}$ is the number of carrier wavelengths between satellite S and receiver r, or integer ambiguity;
δt_{r} is the receiver clock error for carrier phase (s);
δt^{S} is the satellite clock error for carrier phase (s);
$\delta_{\mathrm{r}}^{\mathrm{S}}$ is the multi-path induced errors for carrier phase (m);
$\varepsilon_{\mathrm{r}}^{\mathrm{S}}$ is the carrier phase Gaussian, independent, zero mean random measurement noise (m)

Multiplying (2) by the signal carrier wavelength λ, the following is obtained:

$$\phi_r^s(t_r) = \lambda{\cdot}\varphi_r^{\mathrm{S}}(t_r) = \rho_r^{\mathrm{S}}(t^{\mathrm{S}}) + \lambda{\cdot}N_r^{\mathrm{S}} + c{\cdot}\cdot\,\delta t_r - c{\cdot}\cdot\,\delta t^{\mathrm{S}} - I_r^{\mathrm{S}}(t_r) + T_r^{\mathrm{S}}(t_r) + \delta_r^{\mathrm{S}}(t_r) + \varepsilon_r^{\mathrm{S}}(t_r) \quad (3)$$

As observed in (1) and (3), there are several error sources that affect the code pseudodistance and carrier phase mea-

surement. In order to mitigate their impact in the ambiguity estimation, the difference between measurements from two receivers (single difference) and between two satellites (double difference) can be applied as described in (4), (5), (6), and (7).

Although the multi-path errors can introduce significant errors in the observables (meters for the pseudodistance; and cm for carrier phase), it is known that this parameter is difficult to be modeled, as its characteristics will vary depending on the antenna installation position and the proximity of reflexive surfaces. Therefore, here this parameter will be neglected, i.e.,

$$d_{\mathrm{r}}^{\mathrm{S}} = \delta_{\mathrm{r}}^{\mathrm{S}} = 0 \tag{4}$$

For the single and double differences below, notice that the equations are described for a single-epoch observation, therefore the time tr will be omitted:

$$p_{\mathrm{AB}}^{j} = \rho_{\mathrm{AB}}^{j} + c{\cdot}\mathrm{d}t_{\mathrm{AB}} + I_{\mathrm{AB}}^{j} + T_{\mathrm{AB}}^{j} + e_{\mathrm{AB}}^{j} \tag{5}$$

where

$p_{\mathrm{AB}}{}^{j}$ is the single difference between receiver A and B code data, transmitted from satellite j;
$\rho_{\mathrm{AB}}{}^{j} = \rho_{\mathrm{A}}{}^{j} - \rho_{\mathrm{B}}{}^{j}$ is the difference between geometric distances between satellite j and receivers A and B, respectively;
$\mathrm{d}t_{\mathrm{AB}} = \mathrm{d}t_{\mathrm{A}} - \mathrm{d}t_{\mathrm{B}}$ is the difference between receivers A and B code clock errors;
$I_{\mathrm{AB}}{}^{j} = I_{\mathrm{A}}{}^{j} - I_{\mathrm{B}}{}^{j}$ is the difference between ionospheric induced error on receivers A and B.
$T_{\mathrm{AB}}{}^{j} = T_{\mathrm{A}}{}^{j} - T_{\mathrm{B}}{}^{j}$ is the difference between tropospheric induced error on receivers A and B.
$e_{\mathrm{AB}}{}^{j} = e_{\mathrm{A}}{}^{j} - e_{\mathrm{B}}{}^{j}$ is the difference between receivers A and B code random noises

$$\phi_{\mathrm{AB}}^{j} = \rho_{\mathrm{AB}}^{j} + \lambda{\cdot}N_{\mathrm{AB}}^{j} + c{\cdot}\delta t_{\mathrm{AB}} - I_{\mathrm{AB}}^{j} + T_{\mathrm{AB}}^{j} + \varepsilon_{\mathrm{AB}}^{j} \tag{6}$$

where

$\Phi_{\mathrm{AB}}{}^{j}$ is the single difference between receiver A and B carrier phases, transmitted from satellite j;
$N_{\mathrm{AB}}{}^{j} = N_{\mathrm{A}}{}^{j} - N_{\mathrm{B}}{}^{j}$ is the difference between integer ambiguities from satellite j and receivers A and B, respectively;
$\delta t_{\mathrm{AB}} = \delta t_{\mathrm{A}} - \delta t_{\mathrm{B}}$ is the difference between receivers A and B carrier phase clock errors;
$\varepsilon_{\mathrm{AB}}{}^{j} = \varepsilon_{\mathrm{A}}{}^{j} - \varepsilon_{\mathrm{B}}{}^{j}$ is the difference between receivers A and B carrier phase random noise.

It is readily seen that satellite clock errors do not affect (5) and (6). Moreover, assuming that the distance between receivers is small ($<$ 10 km), which is the case for short baseline configurations, the ionospheric and tropospheric errors can also be canceled in the single-difference equation. Figure 4 presents a schematic of how the single difference is obtained when satellite j is visible to receivers A and B.

$$p_{\mathrm{AB}}^{jk} = \rho_{\mathrm{AB}}^{jk} + e_{\mathrm{AB}}^{jk} \tag{7}$$

where

$p_{\mathrm{AB}}{}^{jk}$ is the double difference between receiver A and B code pseudoranges, transmitted from satellites j and k;
$\rho_{\mathrm{AB}}{}^{jk} = \rho_{\mathrm{AB}}^{j} - \rho_{\mathrm{AB}}^{k}$ is the pseudodistance double difference for satellites j and k and receivers A and B;
$e_{\mathrm{AB}}{}^{jk}$ is the double difference k for code pseudodistance random noise between satellite j and k, and receivers A and B

$$\phi_{\mathrm{AB}}^{jk} = \rho_{\mathrm{AB}}^{jk} + \lambda{\cdot}N_{\mathrm{AB}}^{jk} + \varepsilon_{\mathrm{AB}}^{jk} \tag{8}$$

where

$\Phi_{\mathrm{AB}}{}^{jk}$ is the double difference between receiver A and B carrier phases, transmitted from satellites j and k;
$N_{\mathrm{AB}}{}^{jk} = N_{\mathrm{AB}}^{j} - N_{\mathrm{AB}}^{k}$ is the integer ambiguity double difference for satellites j and k and receivers A and B;
$\varepsilon_{\mathrm{AB}}{}^{jk} = \varepsilon_{\mathrm{AB}}^{j} - \varepsilon_{\mathrm{AB}}^{j}$ is the double difference for carrier phase random noise between satellite j and k, and receivers A and B.

Notice that receivers clock errors are removed from (7) and (8). Figure 5 presents a schematic of the double-difference computation for satellites j and k and receivers A and B.

For the integer ambiguity estimation, Eq. (8) has to be applied for the main receiver (selected by the user) and the secondary receiver, taking into account only satellites observed by both simultaneously.

3 C-LAMBDA Method

The C-LAMBDA method (Teunissen 2007; Wang et al. 2009; Park and Teunissen 2009; Giorge et al. 2010; Giorge and Teunissen 2012) is based on its "nonconstrained" version: LAMBDA (Teunissen 1994; Verhagen 2005) and consists in a least square-based carrier phase ambiguity search algorithm. The method is applied in three steps:

1. The carrier phase ambiguity float solution is computed based on least-squares adjustment;
2. The integer ambiguity is estimated from the float solution, considering the baseline (distance between GNSS antennae) is known;

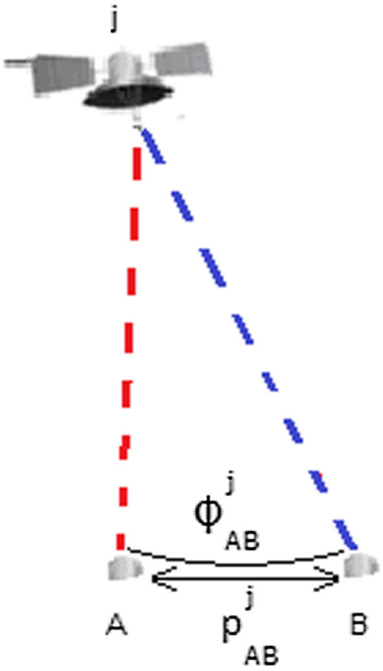

Fig. 4 Single-difference schematics

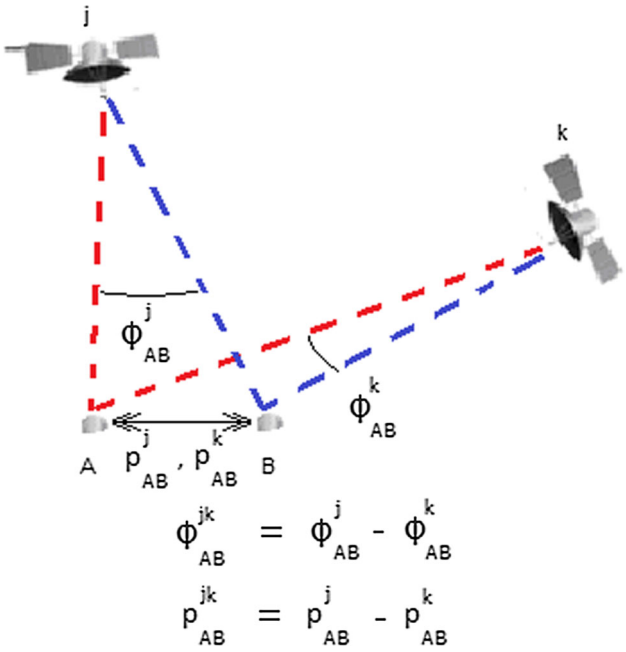

Fig. 5 Double-difference computation schematics

3. The integer ambiguity is used to correct the baseline estimations, obtaining the fixed baseline solution.

The equations that implement the steps above are based on Eqs. (7) and (8) and represent the linearized GNSS observation model below:

$$\underset{m\times 1}{y} = \underset{m\times n}{A}\cdot\underset{n\times 1}{a} + \underset{m\times p}{B}\cdot\underset{p\times 1}{b} + \underset{m\times 1}{e} \tag{9}$$

where

y is the GNSS observation vector, which includes observed minus computed double-differenced phase and/or code pseudorange, on the available signal frequencies;
A and B are design matrix for ambiguity and baseline, respectively;
a is composed of the unknown integer carrier phase ambiguities ($a\epsilon Z^n$);
b is composed of the known baseline increments and may also present additional unknown parameters, such as atmospheric delays ($b\epsilon\Re^p$);

The minimization criteria used to obtain the float initial solutions for a and b (step 1) are given below:

$$\min_{\hat{a},\hat{b}} ||y - A\cdot\hat{a} + B\cdot\hat{b}||^2_{Q_y^{-1}} \tag{10}$$

where

Q_y is the covariance matrix of the observation vector
â is the float solution for the ambiguity
$\hat{b}$ is the initial solution for the baseline vectors

After the ambiguity float solution is obtained, the integer ambiguity is computed based on the following nonlinear quadratically constrained (mixed) integer least-squares minimization problem (Teunissen 2007) (step 2):

$$\begin{aligned}&\min_{\hat{a},\hat{b},\|\hat{b}\|=b_{12}} \|y - A\cdot\hat{a} + B\cdot\hat{b}\|^2_{Q_y^{-1}}\\ &\Rightarrow \min_{a}\left[\|\hat{a} - a\|^2_{Q_{\hat{a}}^{-1}} + \|\hat{b} - b\|^2_{Q_b^{-1},\|b\|=b_{12}}\right]\end{aligned} \tag{11}$$

where b_{12} is the known baseline length between antenna 1 and antenna 2, which will be used as a constraint for the minimization problem.

The solution for (11) requires an integer search procedure in a subset of integer values whose shape and size depend on the covariance matrix Qâ and the search space interval. Equation (12) presents the definition of an ambiguity search space.

$$\Omega_a = \left\{a \in Z^n/(\hat{a} - a)^{\mathrm{T}}\cdot Q_{\hat{a}}^{-1}\cdot(\hat{a} - a) \le \chi^2\right\} \tag{12}$$

where χ^2 is a chosen positive constant that determines the size of the search space.

The C-LAMBDA search space is known to be nonelliptical; therefore, the selection of an appropriate χ^2 can be

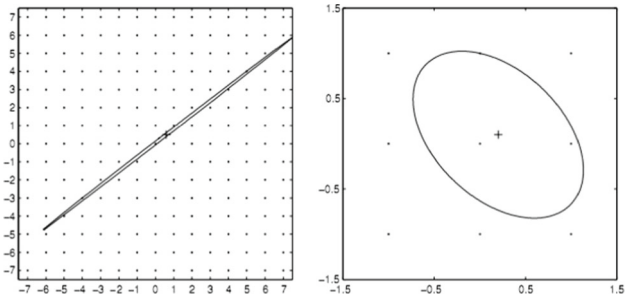

Fig. 6 Original (left) and transformed (right) search spaces—2D example

complex—in Giorge and Teunissen (2012) procedures for this selection are provided.

In order to obtain a less elongated search space shape, the LAMBDA method applies the decorrelation transformation in the ambiguity float solution as follows:

$$\hat{z} = Z^{\mathrm{T}} \cdot \hat{a} \tag{13}$$

$$Q_{\hat{z}} = Z^{\mathrm{T}} \cdot Q_{\hat{a}} \cdot Z \tag{14}$$

$$a = Z^{-T} \cdot z \tag{15}$$

where Z is a volume-preserving transformation matrix composed with integer entries.

The Z-transformed search space is described in (16). Figure 6 presents a two-dimensional example of the significant effect of the transformation in the search space. The time to find an integer solution for (11) is drastically reduced with this procedure (Teunissen 1994).

$$\Omega_z = \left\{ z \in Z^n / (\hat{z} - z)^{\mathrm{T}} \cdot Q_{\hat{z}}^{-1} \cdot (\hat{z} - z) \leq \chi^2 \right\} \tag{16}$$

Using the LDL decomposition for $Q_{\hat{z}}$ simplifies the search for an appropriate z; then through (15), the integer ambiguity a is obtained.

The baseline final solution (step 3) is then fixed as follows:

$$b = \hat{b} - Q_{\hat{b}\hat{a}} \cdot Q_{\hat{a}}^{-1} (\hat{a} - a|) \tag{17}$$

$$Q_b = Q_{\hat{b}} - Q_{\hat{b}\hat{a}} \cdot Q_{\hat{a}}^{-1} \cdot Q_{\hat{a}\hat{b}} \tag{18}$$

where $Q_{\hat{b}\hat{a}}$ and $Q_{\hat{a}\hat{b}}$ are the cross-covariance matrices related to $\hat{b}$ and â; $Q_{\hat{\mathrm{a}}}, Q_{\hat{b}}$ are the covariance matrix of â and $\hat{b}$, respectively.

The search for C-LAMBDA solution candidates is only finished when fixed baseline b (17) satisfies the baseline length constraint and minimizes the cost function. Notice that residual system/model errors are expected, therefore a tolerance of $+-\delta$b should be considered during the baseline constraint evaluation.

After the ambiguity is obtained, an additional validation step is recommended to ensure that the solution is reliable and correct. This can be understood as a "best effort" to prevent a wrong integer solution is selected, but may not be fully efficient if the correct ambiguity has been removed from the search space after the float solution was obtained and the search space was determined. Examples of integer ambiguity validation tests proposed in the literature are the ratio test, the projector test, and the difference test (Verhagen and Teunissen 2006; Giorge et al. 2010).

4 Attitude Based on GNSS Positioning

Considering the high accuracy of the carrier phase-based position determination obtained with at least two GNSS antennae, the body attitude angles can be precisely estimated. This can be done assuming the master antenna as the origin of the body reference system $A_{1,\mathrm{B}} = [0;\ 0;\ 0]_{\mathrm{B}}$ and the second antenna as the reference for one of the body axis. For example, assuming the local level reference system as ENU (East, North, Up), then the second antenna can be arbitrated to be along the body X axis: $A_{2,\mathrm{B}} = [0;\ b12;\ 0]_{\mathrm{B}}$, where b_{12} is the baseline length between antenna 1 and 2.

Considering the rotation sequence: ψ (yaw), θ (pitch), φ (roll), the transformation from body to ENU reference system is given by:

$$D_{\mathrm{ENU}}^{\mathrm{B}} = \lfloor\, D1_{\mathrm{ENU}}^{\mathrm{B}}\ D2_{\mathrm{ENU}}^{\mathrm{B}}\ D3_{\mathrm{ENU}}^{\mathrm{B}} \,\rfloor \tag{19}$$

where

$$D1_{\mathrm{ENU}}^{\mathrm{B}} = \begin{bmatrix} \cos(\phi)\cdot\cos(\psi) - \sin(\phi)\cdot\sin(\theta)\cdot\sin(\psi) \\ \cos(\varphi)\cdot\sin(\psi) + \sin(\varphi)\cdot\sin(\theta)\cdot\cos(\psi) \\ -\sin(\varphi)\cdot\cos(\theta) \end{bmatrix}$$

$$D2_{\mathrm{ENU}}^{\mathrm{B}} = \begin{bmatrix} -\cos(\theta)\cdot\sin(\psi) \\ \cos(\theta)\cdot\cos(\psi) \\ \sin(\theta) \end{bmatrix}$$

$$D3_{\mathrm{ENU}}^{\mathrm{B}} = \begin{bmatrix} \sin(\phi)\cdot\cos(\psi) + \cos(\phi)\cdot\sin(\theta)\cdot\sin(\psi) \\ \sin(\varphi)\cdot\sin(\psi) - \cos(\varphi)\cdot\sin(\theta)\cdot\cos(\psi) \\ \cos(\varphi)\cdot\cos(\theta) \end{bmatrix}$$

So the transformation of antenna 2 position from body frame to ENU is given by:

$$A_{2,\mathrm{ENU}} = D_{\mathrm{ENU}}^{\mathrm{B}} \cdot A_{2,B} \Rightarrow \begin{bmatrix} y_2 \\ x_2 \\ z_2 \end{bmatrix}_{\mathrm{ENU}} = b_{12} \cdot \begin{bmatrix} -\cos(\theta)\cdot\sin(\psi) \\ \cos(\theta)\cdot\cos(\psi) \\ \sin(\theta) \end{bmatrix} \tag{20}$$

Based on (20), ψ and θ can be obtained as follows:

$$\psi = -\tan^{-1}(y_{2,\mathrm{ENU}} / x_{2,\mathrm{ENU}}) \tag{21}$$

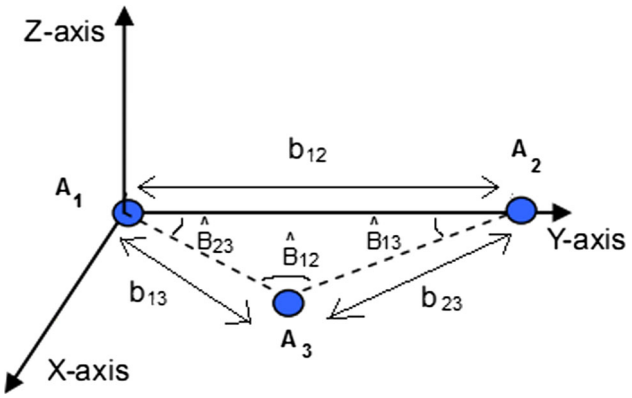

Fig. 7 Antenna reference frame configuration

$$\theta = -\sin^{-1}(z_{2,\mathrm{ENU}}) = \tan^{-1}\left(\frac{z_{2,\mathrm{ENU}}}{\sqrt{x_{2,\mathrm{ENU}}^2 + y_{2,\mathrm{ENU}}^2}}\right) \quad (22)$$

For the computation of the roll angle φ, a third antenna in arbitrary position $A_{3,\mathrm{B}} = [x3;\ y3;\ 0]$ is required. Figure 7 presents the schematic for three antennae configuration and the body frame axis.

Even though it is possible to compute $A_{3,\mathrm{B}}$ position (24) using the baseline lengths b_{13} and b_{23} and applying the cosines law as in (23), the roll angle computation does not require this information to be computed. Applying the yaw R1 and pitch R2 rotations in the $A_{3,\mathrm{ENU}}$ estimated position, the intermediary vector $A_{3,\mathrm{R2.R1}}$ is obtained. This vector is only a roll angle apart from the body reference system. Therefore, the roll angle can be estimated using the third component of $A_{3,\mathrm{ENU}}$ and $A_{3,\mathrm{B}}$ and the roll angle rotation matrix,

$$\hat{B}_{23} = \cos^{-1}\left(\frac{b_{23}^2 - b_{12}^2 - b_{13}^2}{-2{\cdot}b_{12}^2{\cdot}b_3^2}\right) \quad (23)$$

$$A_{3,\mathrm{B}} = [b_{13}{\cdot}\sin(\hat{B}_{23});\ b_{13}{\cdot}\cos(\hat{B}_{23});\ 0]_B \quad (24)$$

$$A_{3,\mathrm{B}} = \begin{bmatrix} \cos(\varphi) & 0 & -\sin(\varphi) \\ 0 & 1 & 0 \\ \sin(\varphi) & 0 & \cos(\varphi) \end{bmatrix} \cdot A_{3,R2{\cdot}R1}$$

$$\Rightarrow \varphi = -\tan^{-1}(z_{3,R2{\cdot}R1}/x_{3,R2{\cdot}R1}) \quad (25)$$

where

$$A_{3,R2{\cdot}R1} = R2{\cdot}R1{\cdot}A_{3,\mathrm{ENU}};$$

$$R1 = \begin{bmatrix} \cos(\psi) & \sin(\psi) & 0 \\ -\sin(\psi) & \cos(\psi) & 0 \\ 0 & 0 & 1 \end{bmatrix};$$

$$R2 = \begin{bmatrix} 1 & 0 & 0 \\ 0 & \cos(\theta) & \sin(\theta) \\ 0 & -\sin(\theta) & \cos(\theta) \end{bmatrix}$$

Although this paper will consider only the above-mentioned attitude determination approach, other methods could also be used in order to estimate the antennae reference system, such as based on least squares, singular value decomposition, or in eigenvalues decomposition. Detailed information on other methods is available in Lu (1995), Shuster and Oh (1981), Mortari (2000).

5 Angle of Sideslip (AOS) and Angle of Attack (AOA)

AOS is associated with aircraft lateral stability and performance (due to drag effect that is introduced in case sideslip cannot be compensated), and AOA is related to longitudinal stability and stall protection.

For $\mathrm{AOS}_{\mathrm{GNSS}}$ (28) and $\mathrm{AOA}_{\mathrm{GNSS}}$ (29) estimation, additional GNSS-derived parameters (besides attitude) must be used: flight path angle γ_{GNSS} (angle of aircraft speed vector in XZ plan—see Fig. 8) and true track angle ζ_{GNSS} (angle of aircraft speed vector azimuth in XY plan—see Fig. 9). Both γ_{GNSS} (26) and ζ_{GNSS} (27) can be directly obtained from receiver computed ground and vertical speeds (Roskam 2001; Etkin 1959).

$$\gamma_{\mathrm{GNSS}} = \frac{[\mathrm{Ground\ Speed}]_{\mathrm{GNSS}}}{[\mathrm{Vertical\ Speed}]_{\mathrm{GNSS}}} \quad (26)$$

$$\zeta_{\mathrm{GNSS}} = [\mathrm{Ground\ Speed\ Direction}]_{\mathrm{GNSS}} \quad (27)$$

$$\mathrm{AOS}_{\mathrm{GNSS}} = \zeta_{\mathrm{GNSS}} - \psi_{\mathrm{GNSS}} \quad (28)$$

$$\mathrm{AOA}_{\mathrm{GNSS}} = \theta_{\mathrm{GNSS}} - \gamma_{\mathrm{GNSS}} \quad (29)$$

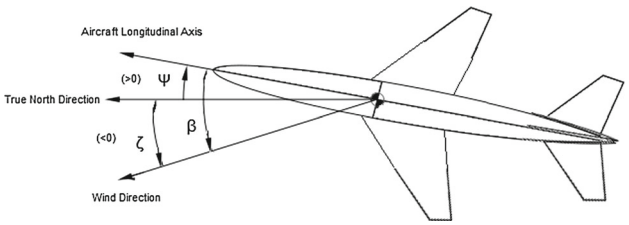

Fig. 8 Angle of sideslip, true track angle, and yaw (or heading)—aircraft upper view

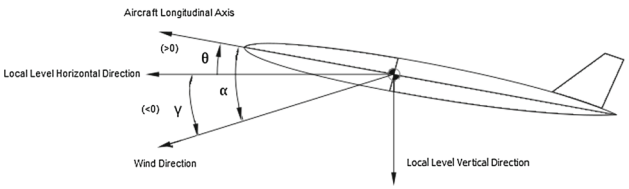

Fig. 9 Angle of attack, flight path angle, and pitch—aircraft side view

6 Results

In this section, the results obtained with real flight data for the GNSS-derived attitude, AOS, and AOA are presented. The (undisclosed) aircraft IRS (inertial reference system) and airdata system (pitot tube and AOS vane and AOA vane) are used as reference for comparison and evaluation of the new proposed application. The satellites configuration is as presented in Fig. 10.

Satellite 28 was the most elevated one during the entire evaluated time spam and therefore was selected as the reference for the double-difference equations. The aircraft has two GPS antennae disposed in such a way that the main one is defined to be at the origin $[0; 0;0]_B$ of the body reference frame, and antenna 2 is placed along body Y axis $[0; b_{12}; 0]$. The known distance between b_{12} antennae was used as constraint for the C-LAMBDA method algorithm.

The aircraft flight profile (ground speed, vertical speed, track angle) is presented in Fig. 11.

6.1 GNSS Attitude Estimation

After inserting the flight data (GPS pseudoranges and phase range) into the C-LAMBDA method as described in Sect. 3, and then calculating the attitude parameters as described in Sect. 4, the results presented in Fig. 12 were obtained. Notice that only 2 GPS antennae are available in this aircraft, therefore only pitch and yaw angles could be estimated.

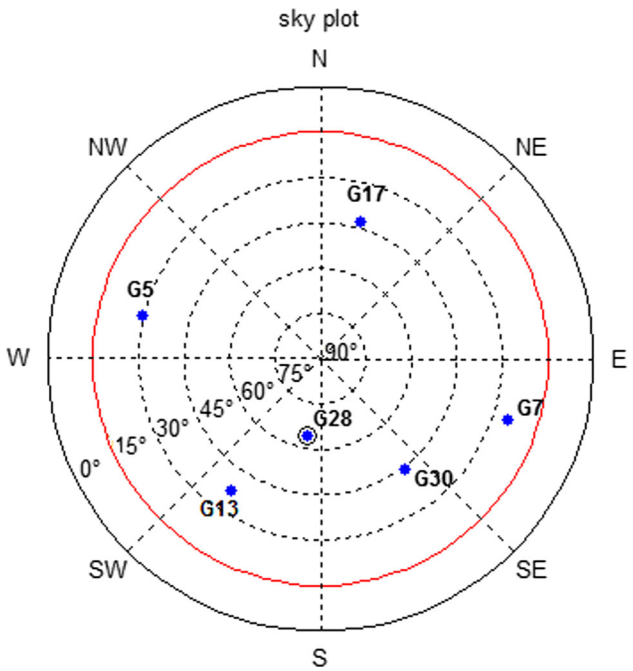

Fig. 10 Sky plot with satellites configuration

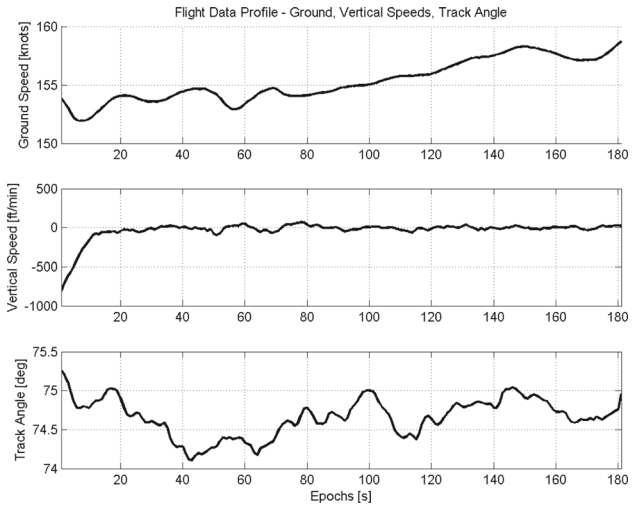

Fig. 11 Flight profile (ground speed, vertical speed, track angle)

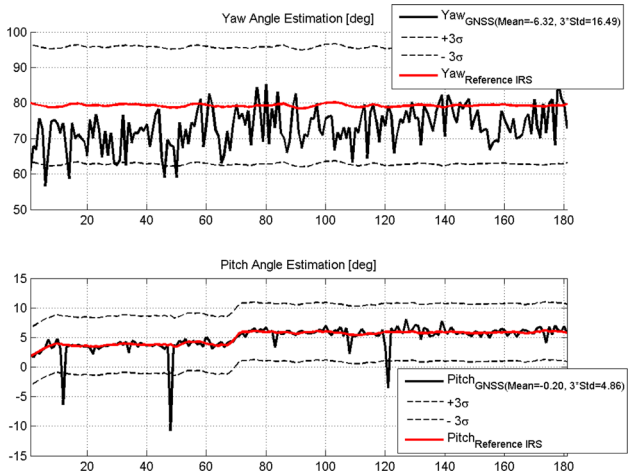

Fig. 12 Attitude estimation using C-LAMBDA method

Yaw angle estimation presented a mean error of $-6.32°$ and 3σ of 16.49°. For pitch angle the obtained values are: $-0.2°$ and 3σ of 4.86°, respectively. Although the yaw angle estimation presented a higher error than pitch angle, the results are considered satisfactory, as the later is more critical than the former in terms of safety.

The high dynamic condition of the flight probably induced errors associated with Doppler effects and also to reflection. The pitch angle "outliers" presented in the time spam could also be easily detected and excluded from the calculation in critical applications.

6.2 GNSS AOS and AOA Estimation

The AOS and AOA are then calculated as described in Sect. 5. As can be observed in Fig. 13, the AOS and AOA behaviors are correlated with yaw and pitch, respectively. Therefore, the viability of the proposed novel application is strongly

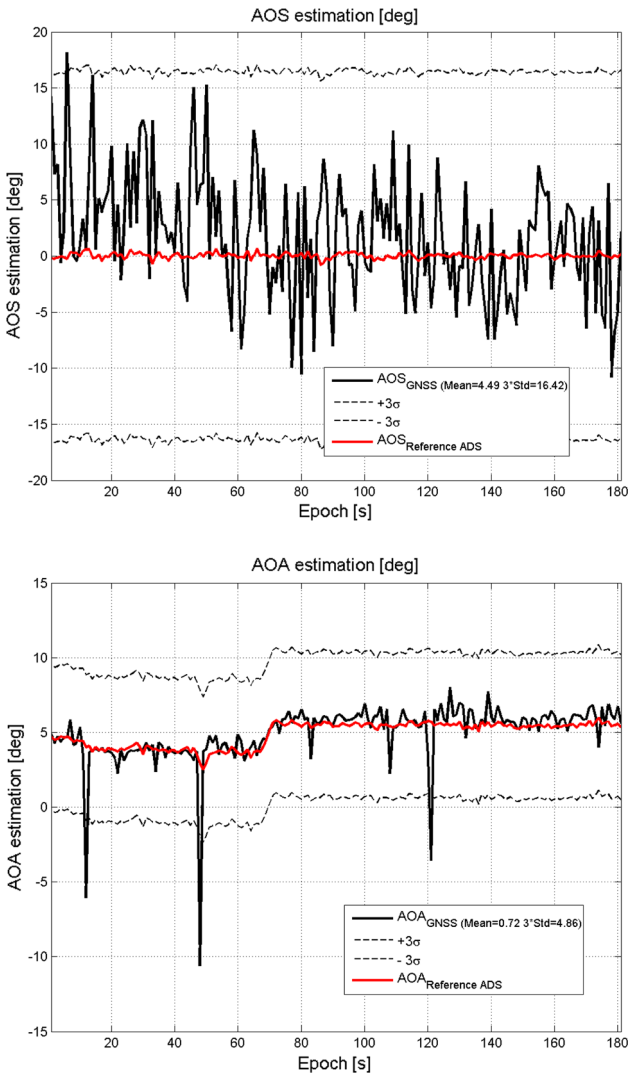

Fig. 13 AOS (above) and AOA (below) estimation

dependent on the reliability of the attitude determination. The results here presented indicate AOS and AOA can be satisfactorily obtained based on this approach. The computed signal could be used for cockpit indications, flight control laws inputs and also for voting purposes (to determine whether any other classical airdata system is failed or unreliable).

7 Conclusion

Currently much effort is being made to improve the GNSS positioning accuracies. In this contribution the GNSS carrier phase-based C-LAMBDA method is applied for a novel aeronautical application that aims to calculate AOS (angle of sideslip) and AOA (angle of attack) in an accurate, independent, dissimilar, low-cost, zero weight, virtually zero power-consuming way.

The method proposed here aims to provide an alternative to avoid integration of several additional, expensive, complex, redundant airdata systems to aircraft due to more restrict icing conditions airworthiness requirements.

Given the known GNSS antennae baseline length, the C-LAMBDA method was shown to produce satisfactory results in terms of accuracy, for yaw and pitch angles. The AOS and AOA could then be computed based on the GNSS attitude solution and also on additional GNSS speeds (ground speed and vertical speed). The AOS and AOA obtained accuracies were similar to the yaw and pitch, respectively. It must be noted that in terms of safety, AOA is more critical than AOS, as it is mainly applied in stall protection control laws. AOS, on the other hand, is important to grant system performance and avoid unwanted drag during flight.

The solution proposed in this paper can virtually be adapted to any aircraft with two or more GNSS antennae whose installation geometry with respect to the vehicle is known. For the novel application to be accepted and implemented in aeronautical industry, a mature and robust solution must be available. For this intent, initial implementation is recommended for instrumentation of experimental/prototype aircraft and UAVs. Then, a software implementation following DO-178C (2012) qualification objectives would allow the solution to be ready for certification.

For future developments and improvements, further investigation on a similar solution combining multiple GNSS technologies (GPS, Galileo, GLONASS, BeiDou, etc.) and multiple frequencies is recommended, as it would improve the ambiguity estimation results and consequently the attitude, AOS, and AOA accuracies. Also using technologies controlled by different countries is beneficial for robustness as it reduces the system dependency. For improving the results, reflection and Doppler effects could also be evaluated in different scenarios so they could be modeled and accounted for during estimation calculations.

References

Bar-Itzhack, I. Y. (1977). Navigation computation in terrestrial strapdown inertial navigation systems. *IEEE Transactions on Aerospace and Electronic Systems, AES*, *13*(6), 679–689.

Baroni, L., & Kuga, H. K. (2009). Evaluation of two integer ambiguity resolution methods for real time GPS positioning. *WSEAS Transactions on Systems*, *8*(3), 323–333.

Baroni, L., & Kuga, H. K. (2012). Analysis of attitude determination methods using GPS carrier phase measurements. *Mathematical Problems in Engineering*, *8*(3), 10.

Chang, X.-W., & Zhou, T. (2006). MILES MATLAB package for solving mixed integer least squares problems, theory and algorithms. *Scientific Computing Laboratory School of Computer Science McGill University*, *11*(4), 289–294.

de F. E. Campos, R. (2011). *Algoritmos de navegação inercial com múltiplas taxas de amostragem para fusão INS/GPS/câmera com*

federação de filtros. Tese de Mestrado em Sistemas e Controle - Instituto Tecnológico de Aeronáutica, São José dos Campos.
DO-178C. (2012). *Software considerations in airborne systems and equipment certification*. Revision C. RTCA.
EDD 2015/08/R. (2015). *Executive director decision certification specifications and acceptable means of compliance for large aeroplanes—CS-25 Amendment 16*. https://www.easa.europa.eu/system/files/dfu/EDDecision2015-008-R.pdf. Accessed January 25 2018.
Etkin, B. (1959). *Dynamics of flight*. New York: Wiley.
Farrel, J. A., & Barth, M. (1999). *The Global Positioning System and Inertial Navigation*. New York: McGraw Hill.
Flottau, J. (2010). *Industry aware of Pitot tube issues since 1995*. Aviation Week. http://aviationweek.com/awin/industry-aware-pitot-tube-issues-1995. Accessed January 25 2018.
Giorge, G., Gourlay, T. P., Teunissen, P. J. G., Huisman, L., & Klaka, K. (2010). *Carrier phase ambiguity resolution for ship attitude determination and dynamic draught*. Australia: FIG Congress.
Giorge, G., & Teunissen, P. J. G. (2012). *GNSS carrier phase-based attitude determination*. Recent Advances in Aircraft Technology, InTech, China.
Groves, P. D. (2008). *Principles of GNSS, inertial, and multisensor integrated navigation systems*. London: Artech House.
Hatch, R. (1990). Instantaneous ambiguity resolution. In *International symposium on kinematic system in geodesy, surveying, and remote sensing* (pp. 299–308), Berlin.
Hermerly, E. M., & Schad, V. R. (2004). *Sistema de Navegação de Baixo Custo Baseado na Fusão INS/GPS Usando Filtro de Kalman*. Gramado, RS: XV Congresso Brasileiro de Automática.
Hofmann-Wellenhof, B., Lichtenegger, H., & Collins, J. (2001). *GPS theory and practice* (5th ed.). Wien: Springer.
Jonge, P., & Tiberius, C. (1996). *The LAMBDA method for integer ambiguity estimation: implementation aspects*. Publications of the Delft Geodetic Computing Centre, LGR-Series, No 12 (p. 173).
Kim, D., & Langley, R. B. (2000). GPS ambiguity resolution and validation: Methodologies, trends and issues. In *7th GNSS Workshop—International symposium on GPS/GNSS* (p. 9), Seoul, Korea.
Leik, A. (1995). *GPS satellite surveying* (2nd ed.). New York: Wiley.
Li, B., & Shen, Y. (2010). Global navigation satellite system ambiguity resolution with constraints from normal equations. *Journal of Surveying Engineering*, *136*(2), 63–71.
Liu, Y., Ge, M., Shi, C., Lou, Y., Wickert, J., & Schuh, H. (2016). Improving integer ambiguity resolution for GLONASS precise orbit determination. *Journal of Geodesy*, *90*(8), 12.
Lopez, M. (2016). *Accidente del Aifrance 447*. Aviacion para Todos. http://aviacionparatodos1.blogspot.com.br/2016/06/accidente-del-aifrance-447.html. Accessed January 29 2018.
Lu, G. (1995). *Development of a GPS multi-antenna system for attitude determination*. PhD. Thesis, University of Calgary, Calgary.
Mortari, D. (2000). Second estimator of the optimal quaternion. *Journal of Guidance, Control, and Dynamics*, *23*(5), 885–888.
Nadarajah, N., Khodabandeh, A., & Teunissen, P. J. G. (2016). *Assessing the IRNSS L5-signal in combination with GPS, Galileo, and QZSS L5/E5a-signals for positioning and navigation*. GPS Solut, No 20 (pp. 289–297).
NPA 2012-22. (2012). *Large aeroplane certification specifications in supercooled large drop, mixed phase, and ice crystal icing conditions—Advisory material*. https://www.easa.europa.eu/system/files/dfu/NPA%202012-22.pdf. Accessed January 25 2018.
Park, C., & Teunissen, P. J. G. (2009). Integer least squares with quadratic equality constraints and its applications to GNSS attitude determination systems. *International Journal of Control, Automation, and Systems*, *7*(4), 566–576.
Quan, Y., Lau, L., Roberts, G. W., & Meng, X. (2016). Measurement signal quality assessment on all available and new signals of multi-GNSS (GPS, GLONASS, Galileo, BDS, and QZSS) with real data. *The Journal of Navigation*, *69*, 313–334.
Roskam, J. (2001). *Airplane flight dynamics and automatic flight controls*. USA: DAR Corporation.
Savage, P. G. (1998a). Strapdown inertial navigation integration algorithm design part I: Attitude algorithms. *Journal of Guidance, Control and Dynamics*, *21*(1), 19–27.
Savage, P. G. (1998b). Strapdown inertial navigation integration algorithm design part II: Velocity and position algorithms. *Journal of Guidance, Control and Dynamics*, *21*(2), 208–221.
Shuster, M. D., & Oh, S. D. (1981). Three-axis attitude determination from vector observations. *Journal of Guidance and Control*, *4*(1), 70–77.
Skybrary. (2018). *Unreliable airspeed indication 2017*. http://www.skybrary.aero/index.php/Unreliable_Airspeed_Indications. Accessed January 25.
Sultan, R. (2015). *Operational impact of §25.1420 and Appendix O*. Federal Aviation Administration.
Teunissen, P. J. G. (1994). *A new method for fast carrier phase ambiguity estimation* (pp. 562–573). IEEE Position Location and Navigation System: Las Vegas.
Teunissen, P. J. G. (2007). The LAMBDA method for the GNSS compass. *Art Satellites*, *41*, 89–103.
Teunissen P. J. G. (2017). *Carrier phase integer ambiguity resolution*. Springer handbook of global navigation satellite systems (1st ed., pp. 661–685).
Teunissen, P. J. G., Giorgi, G., & Buist, P. J. (2011). Testing of a new single-frequency GNSS carrier phase attitude determination method: Land, ship and aircraft experiments. *GPS Solutions*, *15*, 15–28.
Titterton, D. H., & Weston, J. L. (1997). *Strapdown inertial navigation technology*. London: Peter Perigrinus Ltd.
Verhagen, S. (2005). *The GNSS integer ambiguities estimation and validation*. Delft Institute of Earth Observation and Space Systems, Delft University of Technology phD thesis.
Verhagen, S., & Teunissen, P. J. G. (2006). New global navigation satellite system ambiguity resolution method compared to existing approaches. *Journal of Guidance, Control, and Dynamics*, *29*(4), 981–991.
Wang, B., Miao, L., Wang, S., & Shen, J. (2009). A constrained LAMBDA method for GPS attitude determination. *GPS Solutions*, *13*, 97–107.